LANGMUIR

pubs.acs.org/Langmuir Article

Surfactant Adsorption to Gypsum Surfaces and the Effects on Solubility in Aqueous Solutions

Galip Yiyen, Kodie V. Duck, and Robert A. Walker*



Cite This: Langmuir 2022, 38, 2804-2810



ACCESS

Metrics & More

Article Recommendations

Supporting Information

Carbon

Carbon

Carbon

Carbon

Added BaCl, (mmoles)

ABSTRACT: Vibrational sum frequency generation (VSFG) spectroscopy, conductometric titration measurements, and EDX elemental mapping were used to examine surfactant adsorption to the gypsum (010) surface and assess the effects of surfactant adsorption on gypsum solubility in aqueous solutions. Sodium dodecyl sulfate (SDS) and dodecyltrimethylammonium chloride (DTAC) were used as anionic and cationic surfactants, respectively. Gypsum/SDS interactions result in an ordered precipitate layer on the gypsum surface after water evaporation; gypsum/DTAC interaction did not show a similar effect, despite exposure of gypsum to equivalent amounts of surfactant. VSFG spectra showed that SDS molecules adsorb with their chains parallel to the gypsum surface; spectra from gypsum surfaces treated with DTAC, however, showed no measurable response, implying that these surfactants form disorganized aggregates with no polar ordering. Vibrational data were supported by independent EDX measurements that show a uniform distribution of SDS across the gypsum surface. In contrast, element-specific EDX images showed that DTAC clustered in tightly localized patches that left most of the gypsum surface exposed. The uniform adsorption of SDS on the gypsum surface suppresses long-term dissolution up to 40% when compared to samples exposed to DTAC. Gypsum samples in DTAC-containing solutions lose approximately the same amount of material to dissolution as samples immersed in pure water.

■ INTRODUCTION

Surfactant adsorption to mineral surfaces is a proven strategy used to control conformationally directed crystal growth and mineral dissolution. Prevailing wisdom posits that surfactants adsorb preferentially to different crystalline faces, slowing growth along specific directions and leading to anisotropic growth/dissolution. As a synthetic strategy, varying surfactant identity and concentration can change particle aspect ratios and shape. Neutral surfactants such as polyvinylpyrrolidone (PVP) are used to control particle size in seeded solutions, while charged surfactants including sodium dodecyl sulfate (SDS) and dodecyltrimethylammonium bromide (DTAB) are often added to particle-containing solutions to modify oxide surface properties for applications such as enhanced oil recovery and pollutant remediation. See

Surfactant adsorption to minerals also underpins the practice of froth flotation and mineral recovery. In this process, hydrophilic but sparingly soluble minerals are rendered hydrophobic by first pulverizing the ore (to create particles

with diameters \leq 100 μ m), suspending the particles in a slurry, and then treating the slurry with a surfactant that binds selectively to the material of choice, forcing those particles to float to the surface. The froth is collected, and the desired mineral is cleaned and isolated. The success of froth flotation hinges on choosing surfactants that bind preferentially to specific mineral surfaces at the exclusion of others. While this process has been employed commercially for well over a century, the development of suitable surfactants and surfactant mixtures has proceeded largely through empirical testing rather than predictive design. 10,11

Received: October 29, 2021 Revised: February 17, 2022 Published: February 28, 2022





To describe froth flotation, models have been developed to describe how mineral particle properties should depend on variables such as surfactant surface coverage and particle size,1 but few studies have considered the structure and organization of the adsorbed surfactants themselves. 12-19 Such information is critical for understanding the stability of mineral-aqueous interfaces as well as mineral wetting and hydration. Given the increasing importance of surfactant-mineral interactions in both technological and environmental applications, efforts to identify—and even design from computational predictions²⁰ surfactants that bind mineral surfaces efficiently are expected to intensify. In this context, testing predictions and validating proposed models with independent, complementary methods will be indispensable for informing and refining mineral recovery and environmental remediation strategies. Studies described below use surface-sensitive vibrational spectroscopy coupled with ex situ EDX imaging and bulk solution conductometric titrations to examine SDS and dodecyltrimethylammonium chloride (DTAC) adsorption to gypsum (CaSO₄·2H₂O) surfaces and the impact that surfactant adsorption has on gypsum solubility in aqueous solution.

Gypsum is an earth abundant mineral commonly found in sedimentary rock deposits. Commercially, gypsum has many uses including as a building material, as an additive that regulates cement behavior, and as a fertilizer/soil conditioner. Despite its many benefits, however, gypsum is also a source of sulfate in ground and surface water, and gypsum dissolution has been correlated to rising sulfate levels in rivers and wetlands, especially in areas containing construction and demolition debris²¹ as well as naturally occurring Karst mineral deposits. 22,23 Sulfate is also a common inorganic fouling agent that poses problems for reverse osmosis systems.²⁴ The EPA has set a secondary maximum contaminant level of 250 mg/L SO₄²⁻ for potable drinking water. At higher sulfate concentrations, contaminated water is no longer suitable for agricultural applications, and concentrations above 3000 mg/L can lead to neurological damage in livestock.²⁸

As a mineral commonly found in limestone, sandstone, and other sedimentary rock formations, gypsum has ample opportunity to contribute to groundwater and surface water salinity.²⁶ Recent studies have reported that adding sodium sulfate to the injected solutions used in oil recovery applications slows the rate of gypsum dissolution. 27,28 Here, the efficacy of additives in preventing gypsum dissolution is assessed by measuring surfactant concentrations in the system effluent and then calculating how much surfactant has been retained.²⁹ Mechanisms responsible for surfactant-induced retention, however, remain speculative. Results described below show that SDS interacts strongly with gypsum, forming ordered films with surfactant chains aligned with their long axes parallel to the surface. In contrast, equivalent amounts of a cationic surfactant, DTAC, aggregate in a disordered fashion in patches on the gypsum surface, leaving large areas of the mineral fully exposed. These behaviors affect gypsum dissolution properties. Gypsum in DTAC-containing solutions (4 mM) dissolves to the same extent as in pure, Millipore water (pH = 5.8), but SDS-containing solutions (4 mM) suppress gypsum dissolution by ~40%. Taken together, these findings present a clear and compelling picture of how two common surfactants associate with an environmentally and economically important mineral surface. These findings motivate additional experimental work and computational simulations to identify chemically specific forces that control

molecular adsorption and organization in hydrogeological systems.

MATERIALS AND METHODS

Sample and Solution Preparation. Gypsum samples were purchased from Kidz Rocks, Inc. The outer layers of crystal were cleaved with a razor to access clean (010) surfaces. The gypsum pieces used for VSFG and FTIR measurements were approximately 1 cm \times 1 cm and 3 mm thick; samples used for EDX measurements were smaller, approximately 0.5 cm \times 0.5 cm and less than 1 mm thick. To assess the ability of surfactants to organize on a gypsum surface, approximately 2.5×10^{-7} mol of SDS and DTAC in aqueous solutions (\sim 150 μ L) was applied to the (010) gypsum surfaces, and these surfaces were then dried under clean air for 2 h before performing VSFG and EDX measurements.

Sodium dodecyl sulfate (SDS, ACS reagent, ≥99.0%) and dodecyltrimethylammonium chloride (DTAC, ≥99.0%) were purchased from Sigma-Aldrich. All chemicals were used without further purification. Structures of these molecules are shown in Figure 1.

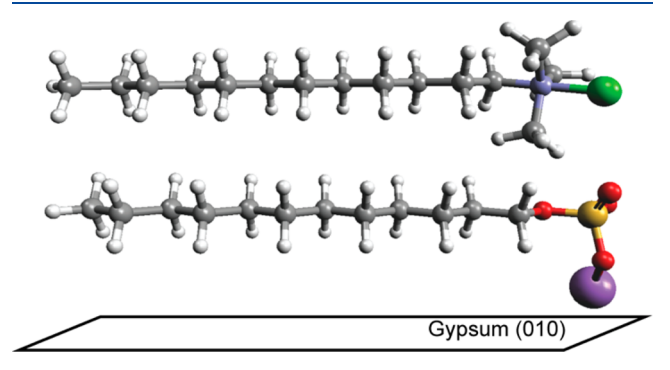


Figure 1. Ball and stick structures for both SDS (below) and DTAC (above) molecules. Both surfactants are in all-trans conformations. Structures include each surfactant counterion (Na⁺ (purple) for SDS and Cl⁻ (green) for DTAC). Note that while the SDS solute is shown in a geometry consistent with findings from VSFG measurements (vide infra), DTAC adsorbed to the gypsum surface shows no evidence of surface-induced ordering.

Millipore water (resistivity 18.2 $M\Omega)$ was used to prepare the 4 mM SDS and 4 mM DTAC solutions. Solution pH was unbuffered and measured 5.8–6.0. Modest changes in surfactant concentration (2 and 6 mM) led to no discernible changes in the observed results. Given a reported point of zero charge (PZC) in aqueous solutions between pH = 2–3, 30 we expect that the gypsum surface in these solutions will carry a net negative charge.

Conductometric Titrations. Conductometric titrations are a means for determining the amount of analyte dissolved in solution by observing the change in solution conductivity as a complexing agent is added. In this study, the amount of sulfate from gypsum dissolution was determined in pure water and solutions containing either SDS or DTAC. The important principle in conductometric titration is to choose a titrant having high solubility by itself but having a very low solubility product with the dissolved analyte of interest. We chose BaCl₂ as the titrant so that in SO_4^{2-} -containing solutions BaSO₄ would precipitate $(K_{SP} = 1.1 \times 10^{-10})$. As long as a precipitate continues to form, the solution conductivity decreases. Once all of the analyte has precipitated, further addition of the titrant results in an increase in solution conductivity. The minimum in solution conductivity represents the titration's end point. Tests with laboratory-prepared standards showed that this technique is ≥95% accurate with typical variation of ≤2.5% about the mean.

EDX Mapping. EDX images were acquired by using a PHI 710 Auger NanoProbe. Gypsum pieces were mounted on a tilted (30°) sample holder. To minimize surface charging, gypsum samples were

irradiated with low-energy ions (\sim 70 eV) from an Ar $^+$ sputtering gun. The ion beam energy used for analyses was 5 keV.

FTIR Analysis. Gypsum pieces $(1~cm \times 1~cm)$ were immersed in 4 mM SDS and DTAC solutions for up to 5 days. The DTAC solution remained clear, but the SDS solution became cloudy within 1 day. The precipitate observed in gypsum/SDS solutions was dried under clean air on a ZnSe window so that IR absorption experiments could be performed.

All FTIR measurements were performed with a Bruker VERTEX 70. Spectra were collected between 400 and 7000 cm⁻¹ and were composed of an average of 32 scans with 1 cm⁻¹ resolution.

Vibrational Sum Frequency Generation. Vibrational sum frequency generation (VSFG) spectroscopy is a second-order, nonlinear optical technique used to measure vibrational spectra of molecules at interfaces. In order for vibrational transitions to be VSF allowed, they must be both IR- and Raman-active and in an anisotropic environment. Molecules in bulk materials having inversion symmetry or in solution will not give rise to a VSF response. Similarly, adsorbates that are randomly distributed and/or disordered at a surface will also be VSF silent. Additional information about VSFG as a technique can be found in several instructive reviews. 34–36

VSFG data presented in this work were acquired by using an assembly previously described. $^{37-39}$ Briefly, the 800 nm output from an amplified Ti:sapphire laser (3.4 W, 1 kHz, 85 fs) (Coherent Libra-HE) was split so that 80% of the intensity was used to pump a Coherent OPerA Solo that was tuned to produce IR light centered in the –CH stretching region (3400 nm, \sim 200 cm $^{-1}$ bandwidth). The remaining 800 nm light was spectrally narrowed with a home-built pulse shaper to have an \sim 15 cm $^{-1}$ FWHM. Visible and IR beams were focused on the air–solid interface for 60 s for each measurement, and the VSF signal was collected with a 1340 \times 100 pixel CCD (PIXIS100B, Princeton Instruments). Typical visible and IR powers were 50 and 20 mW, respectively. Band intensities were normalized to the corresponding nonresonant response from a gold surface. 40

RESULTS AND DISCUSSION

Conductometric Titration. Gypsum pieces with varying masses were placed in aqueous and surfactant containing solutions and allowed to sit for 5 days. The pieces were then removed from solution and aliquots from these solutions were titrated with BaCl₂. Sulfate concentrations in different solutions were found by determining the end points of conductometric titration curves. For each sample, the amount of sulfate in solution was normalized by the mass of the parent gypsum piece prior to immersion. Even prior to the titration analysis, clear differences between the solutions were apparent. While gypsum/DTAC and gypsum/Millipore solutions remained clear after 5 days, the gypsum/SDS solution was extremely cloudy and particles in the precipitate were visible to the naked eye. Following this observation, a solution with CaCl₂ and SDS was prepared, and similar precipitation behavior was observed immediately. Previous work has reported Ca(DS)₂ precipitation as a result of an interaction between Ca²⁺ and SDS anions in solution. 41,42 Baviere et al. reported that in a solution with dodecyl sulfate concentration at 4 mM Ca(DS)₂ precipitation was observed with Ca²⁺ concentrations varying from 0.02 to 7 mM.⁴³

Representative results from conductometric titrations performed with the Millipore, DTAC, and SDS solutions are shown in Figure 2. In these plots, dashed lines represent titration end points after analyzing the data with nonlinear regressions. Results from repeated measurements were normalized to the original gypsum masses and are reported in Table 1 (expressed in terms of percent material dissolved). Data show less free sulfate in the SDS-containing solutions compared to DTAC (4 mM) and Millipore solutions. These

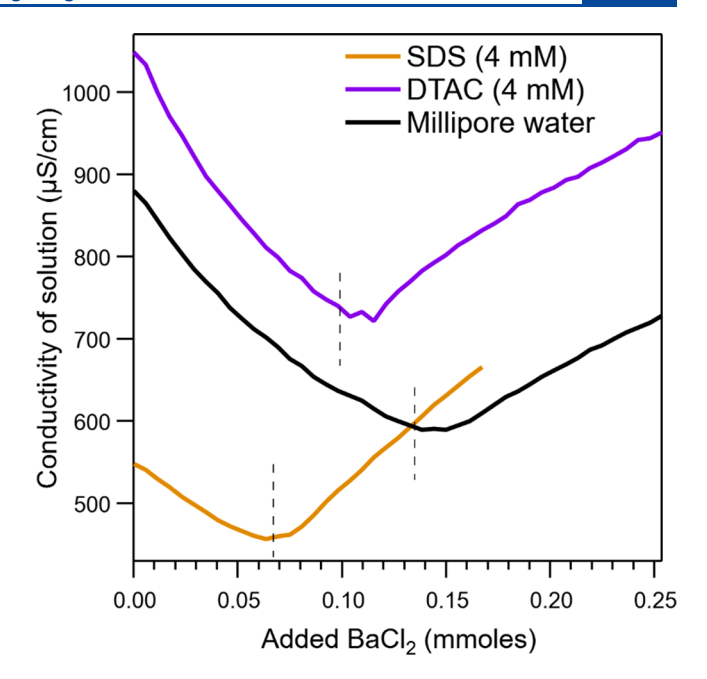


Figure 2. Sample titration curves from each titration set.

Table 1. Percentage of Amount of Sulfate Found in Different Solutions after Normalized to Mass of Gypsum Pieces before Dissolution

type and number of samples	amount of sulfate normalized to mass of gypsum before dissolution (%)	standard deviation (%)
SDS (4 mM), n = 5	5.34	1.3
DTAC (4 mM), $n = 3$	8.37	2.4
Millipore water, $n = 6$	9.00	0.5

findings show that SDS suppresses dissolution by ${\sim}40\%$ relative to pure water and solutions containing the cationic DTAC. By converting the dissolved material into molar quantities, we estimate the sulfate concentrations in the solutions range from 260 mg/L (SDS) to 530 mg/L (DTAC and Millipore).

We note that the amount of free sulfate determined from the conductometric titrations with SDS solutions is an upper limit. Ba²⁺ forms a precipitate not only with SO₄²⁻ but also with the sulfate headgroup on SDS. To confirm this effect, a 3.5 mM SDS solution (e.g., no free dissolved sulfate) was titrated with BaCl₂ as a control measurement. As expected, a stoichiometric analysis of the data showed that each barium cation complexed with two dodecyl sulfate groups and precipitated. In other words, if Ba²⁺ precipitates primarily with free sulfate but also with any remaining SDS that remains uncomplexed with dissolved Ca2+, then the end point in the conductometric titrations will represent the amount of Ba2+ required to complex with SO₄²⁻ and SDS, meaning that the calculated amount of free sulfate will be greater than the actual amount in solution. As a result, we conclude that gypsum solubility in the SDS solution is significantly less than in solutions of pure Millipore water and solutions containing the cationic surfactant DTAC.

VSFG. Gypsum pieces with 1 cm × 1 cm dimensions were placed on a sample stage, and VSFG spectra were collected

from freshly cleaved samples and samples that had been exposed to both SDS and DTAC solutions and had been allowed to dry. Figure 3 shows VSFG spectra acquired in the

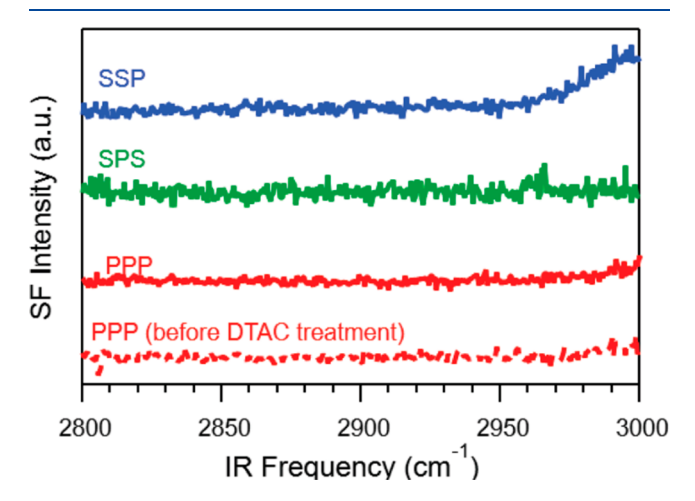


Figure 3. VSFG spectra from gypsum surface before and after treatment with 4 mM DTAC. Spectra were offset vertically for clarity.

CH stretching region under different polarization conditions from a freshly cleaved gypsum (010) surface and one that was treated with ~150 μ L of a 4 mM DTAC solution. No signal was observed from either sample, regardless of experimental polarization conditions. However, treating a gypsum surface with an equivalent volume of 4 mM SDS led to a visibly observable precipitate layer on the surface and relatively strong VSFG signals (Figure 4).

Several different scenarios can lead to an absence of VSFG signal from a surface. First, if no species with appropriate functional group vibrations are present, no response is expected. Second, if species having vibrational structure in the region of interest *are* present but disorganized, the functional groups will experience no net anisotropy and the corresponding second-order susceptibility ($\chi^{(2)}$) will be zero. Finally, if adsorbates *are* ordered but organized in a way that is symmetric with respect to inversion, functional group hyperpolarizabilities will be out of phase leading to cancellation and, again, no detectable VSFG response. The absence of any signal from the DTAC-treated gypsum surface leads us to believe that the surfactant remaining after solvent evaporation are disordered.

In contrast to the gypsum/DTAC experiments, VSFG spectra from a gypsum surface treated with SDS show distinct, complementary features under SSP, SPS, and PPP polarization conditions (Figure 4). In total, four distinct vibrational bands appear corresponding to a methylene symmetric stretch (d⁺, 2850 cm $^{-1}$), a methylene antisymmetric stretch (d $^{-}$, 2920 cm $^{-1}$), and a methyl antisymmetric stretch (r $^{-}$, 2960 cm $^{-1}$). The d $^{-}$ feature is broad and likely contains contributions from methyl bending Fermi resonance overtones. 44,45

While these features are common to VSFG spectra of alkyl chain-containing species, 46,47 the relative band intensities as a function of sum, visible, and IR polarizations are unusual in the SDS on gypsum spectra. The dominant d⁻ intensity in the SSP spectrum implies that surfactant chains are lying parallel to the surface with the local methylene C_2 -axes also parallel to the surface. This picture is supported by the SPS spectrum and relevant vibrational band intensities. Specifically, if alkyl chains

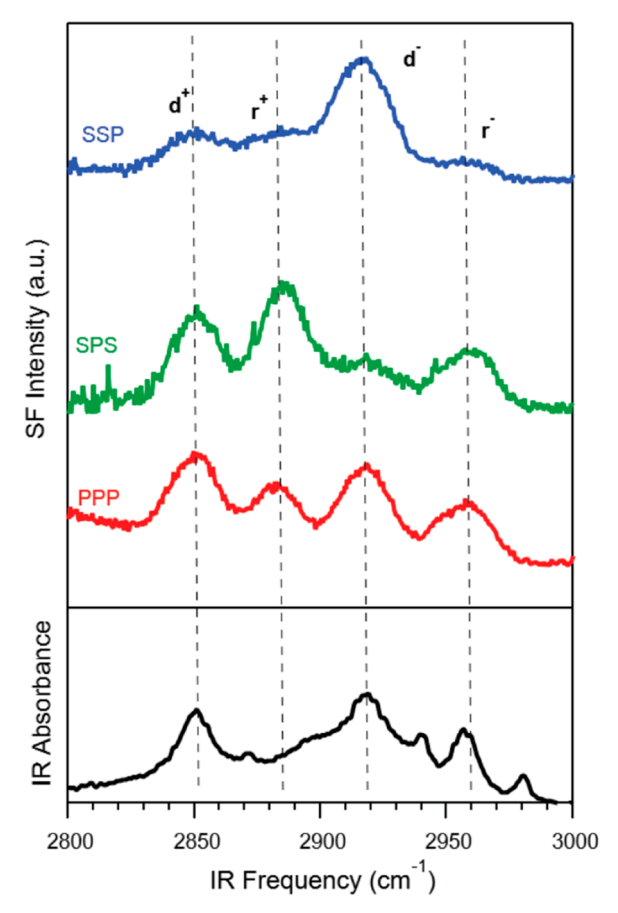


Figure 4. VSFG spectra from gypsum surface before and after treatment with 4 mM SDS and FTIR absorbance spectrum of the precipitate isolated from gypsum/SDS solution. VSFG spectra were offset vertically for clairty. Dashed vertical lines are included as visual guides.

were lying down with each methylene group in contact with the surface (and each local methylene C_2 -axis parallel to the surface), then symmetry conditions lead one to expect a measurable d^+ response under SPS polarization conditions. Similarly, one can also anticipate such an arrangement to lead to a strong r^+ signal under SPS conditions. Inspection of the spectra in Figure 4 shows these expectations fulfilled. Similar observations have been reported recently by Bryantsev and coworkers, who used predictions from computational studies to design and then study strongly binding bis(phosphinate) ligands adsorbed to rare-earth-containing bastnäsite samples.

Figure 4 also shows an FTIR absorbance spectrum of the precipitate collected and dried from gypsum/SDS solution. In general, vibrational features appearing in the VSFG spectra match well with features in the FTIR absorbance spectrum. We note that the FTIR spectrum does contain additional features at 2940 and 2980 cm⁻¹ although these may be obscured in the VSFG data by the poorer (\sim 20 cm⁻¹) resolution. We also observe that the r⁺ feature in the SPS and PPP VSFG spectra is blue-shifted (2884 cm⁻¹) relative to the equivalent band assigned in the FTIR spectrum (2872 cm⁻¹). Computational studies predict that strong interactions between methyl groups and halide anions can lead to CH stretching vibrations shifting to higher frequencies.⁴⁸ Given the daily calibration performed with the VSFG assembly, we believe the r+ shift observed in Figure 4 is real and may reflect the methyl group interacting directly with sulfate anions on the gypsum surface. We

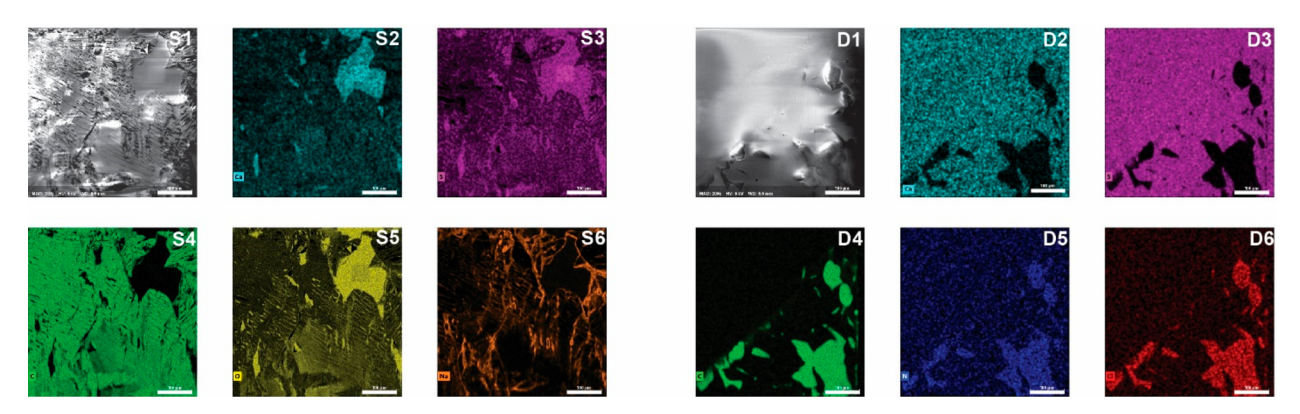


Figure 5. EDX images captured from surfaces of two gypsum pieces after SDS treatment (S1 to S6) and DTAC treatment (D1 to D6). The scale bar represents 100 μ m. Panels S2 and D2 show Ca, panels S3 and D3 show S, panels S4 and D4 show C, panel S5 shows oxygen, panel D5 shows N, panel S6 shows Na, and panel D6 shows Cl.

emphasize, however, that this hypothesis is speculative and in need of testing.

Summarizing the VSFG results, we conclude that DTAC does not interact strongly with the gypsum surface and the cationic surfactant left behind after solvent evaporation forms disordered aggregates with no net polar ordering. In contrast, an equivalent amount of SDS does adsorb to gypsum, effectively "wetting the surface" and creating surface structures that have long-range order and a correspondingly strong VSFG response. Furthermore, the SDS alkyl chains appear to have a well-defined structure relative to the surface, with the chains lying flat and the local C_2 symmetry axes of methylene groups parallel to the surface. We infer that the interactions between the chains and the surface as well as between the chains themselves minimize the amount of intramolecular motion given the relatively strong intensities of both d⁺ and r⁺ in the SPS spectrum.⁴⁹ On the basis of results from conductometric titrations, we infer that these strong gypsum-SDS interactions disrupt water structure at the surface and impede gypsum dissolution. In a global sense, these results support an adsorption mechanism where species specific binding (-OSO₃⁻ of the SDS to the Ca²⁺ on the gypsum surface) is strong enough to overcome the overall negative charge associated with this material surface at an experimental pH of 6.

EDX. To learn more about surfactant structure and organization at the gypsum/air interface, we acquired EDX images from gypsum that had been treated with either SDS or DTAC. Figure 5 shows EDX images of element distributions across the surfaces of gypsum pieces treated with solutions containing 4 mM SDS (left) and DTAC (right).

Following exposure to the surfactant containing solutions, the aqueous solvent was allowed to evaporate for 2 h under a stream of clean air. For the SDS-treated surface, elemental mapping shows a relatively uniform carbon distribution across the surface (S4). Furthermore, we observe calcium only at the site/defect where carbon is absent (S2). The other unique diagnostic from the SDS treated surface is the distribution of Na that also appears across the surface in filamentous-like pattern (S6). Closer inspection of Figure S4 (carbon) and Figure S5 (oxygen) shows 8–12 μ m length striations in the elemental distributions implying a degree of organization within the adsorbed surfactants, consistent with conclusions drawn from the VSFG results reported above.

In contrast, the unique indicators of DTAC on the gypsum surface—carbon, nitrogen, and chlorine—are all spatially correlated to each other, and their distributions are localized to a small areas within the 0.5 mm × 0.5 mm field of view. We note the same elemental exclusion effects observed for the SDS-treated sample, namely, that in combination with the raw SEM image (D1) the DTAC elemental distributions show that the cationic surfactant assembled at the topographically rough patch of the gypsum surface, and the surfactant did not have a strong enough affinity for spread across the substrate. Again, this result is consistent with VSFG spectra that implied no net DTAC polar ordering across the gypsum surface.

CONCLUSIONS

In an effort to understand experimental conditions that affect gypsum dissolution into aqueous solution, conductometric titrations demonstrated that solutions containing the anionic surfactant SDS at submicellar concentrations measurably suppressed gypsum dissolution while a corresponding cationic surfactant, DTAC, had no measurable impact. Subsequent surface specific vibrational experiments showed that gypsum surfaces exposed to SDS solutions where the solvent was then allowed to evaporate were covered with an ordered surfactant film where the alkyl chains adopted a conformation with their long axes approximately parallel to the surface plane. In contrast, gypsum exposure to a DTAC-containing solution showed no such polar ordering among the surfactants. Complementary EDX images confirmed conclusions drawn from the vibrational data by revealing a uniform carbon coating across the gypsum surface that had been treated with SDS. The DTAC-treated surface showed all of the carbon collected in localized patches, leaving large expanses of the gypsum surface uncoated.

One suggestive consequence emerging from the findings reported in this work is that the well-ordered, long-range organization created by SDS surfactants adsorbing to the aqueous/gypsum interface is that the now-hydrophobic gypsum surfaces may disrupt water structure and limit gypsum solubility. Such molecular level insight would provide meaningful data for models being developed to predict the environmental impact of organic matter adsorbed to mineral surfaces.

ASSOCIATED CONTENT

5 Supporting Information

The Supporting Information is available free of charge at https://pubs.acs.org/doi/10.1021/acs.langmuir.1c02890.

Representative VSFG spectra showing the -OH stretching region from DTAC- and SDS-treated gypsum; FTIR spectra of the pure surfactants emphasizing their vibrational structure in the -CH stretching region (PDF)

AUTHOR INFORMATION

Corresponding Author

Robert A. Walker — Department of Chemistry and Biochemistry and Montana Materials Science Program, Montana State University, Bozeman, Montana 59717, United States; orcid.org/0000-0002-0754-6298; Email: rawalker@montana.edu

Authors

Galip Yiyen – Department of Chemistry and Biochemistry, Montana State University, Bozeman, Montana 59717, United States

Kodie V. Duck – Department of Chemistry and Biochemistry, Montana State University, Bozeman, Montana 59717, United States

Complete contact information is available at: https://pubs.acs.org/10.1021/acs.langmuir.1c02890

Funding

This material is based upon work supported in part by the National Science Foundation EPSCoR Cooperative Agreement OIA-1757351. Any opinions, findings, and conclusions or recommendations expressed in this material are those of the author(s) and do not necessarily reflect the views of the National Science Foundation.

Notes

The authors declare no competing financial interest.

ACKNOWLEDGMENTS

The authors gratefully acknowledge Dr. Toby Koffman in Montana State University's Environmental Analytical Laboratory for performing ICP-MS measurements to test the accuracy of the conductometric titration data. The authors also thank Mr. Seth Kane for his assistance in performing the ATR-FTIR measurements of the SDS and DTAC surfactant powders reported in the Supporting Information.

REFERENCES

- (1) Su, Y.; Li, H. F.; Ma, H. B.; Robertson, J.; Nathan, A. Controlling Surface Termination and Facet Orientation in Cu₂O Nanoparticles for High Photocatalytic Activity: A Combined Experimental and Density Functional Theory Study. *ACS Appl. Mater. Interfaces* **2017**, 9 (9), 8100–8106.
- (2) Shen, Q.; Wang, L. C.; Huang, Y. P.; Sun, J. L.; Wang, H. H.; Zhou, Y.; Wang, D. J. Oriented aggregation and novel phase transformation of vaterite controlled by the synergistic effect of calcium dodecyl sulfate and *n*-pentanol. *J. Phys. Chem. B* **2006**, *110* (46), 23148–23153.
- (3) Shen, Q.; Wei, H.; Wang, L. C.; Zhou, Y.; Zhao, Y.; Zhang, Z. Q.; Wang, D. J.; Xu, G. Y.; Xu, D. F. Crystallization and aggregation behaviors of calcium carbonate in the presence of poly-(vinylpyrrolidone) and sodium dodecyl sulfate. *J. Phys. Chem. B* **2005**, *109* (39), 18342–18347.

- (4) Karimi, M.; Al-Maamari, R. S.; Ayatollahi, S.; Mehranbod, N. Wettability alteration and oil recovery by spontaneous imbibition of low salinity brine into carbonates: Impact of Mg2+, SO42- and cationic surfactant. *J. Pet. Sci. Eng.* **2016**, *147*, 560–569.
- (5) Li, G.; Guo, S. H.; Hu, J. X. The influence of clay minerals and surfactants on hydrocarbon removal during the washing of petroleum-contaminated soil. *Chemical Engineering Journal* **2016**, 286, 191–197.
- (6) Zhao, S. F.; Li, Y. P.; Cao, Z. L.; Wang, J. L. Sorption-desorption mechanisms and environmental friendliness of different surfactants in enhancing remediation of soil contaminated with polycyclic aromatic hydrocarbons. *Journal of Soils and Sediments* **2020**, 20 (7), 2817–2828.
- (7) Sis, H.; Chander, S. Reagents used in the flotation of phosphate ores: a critical review. *Minerals Engineering* **2003**, *16* (7), 577–585.
- (8) Nicol, S. K.; Galvin, K. P.; Engel, M. D. Ion floatation Potential applications to mineral processing. *Minerals Engineering* **1992**, *5* (10–12), 1259–1275.
- (9) Zhang, N. N.; Nguyen, A. V.; Zhou, C. C. A review of the surface features and properties, surfactant adsorption and floatability of four key minerals of diasporic bauxite resources. *Adv. Colloid Interface Sci.* **2018**, 254, 56–75.
- (10) Chang, Z. Y.; Chen, X. M.; Peng, Y. J. The adsorption behavior of surfactants on mineral surfaces in the presence of electrolytes A critical review. *Minerals Engineering* **2018**, *121*, *66*–76.
- (11) Xu, L. H.; Tian, J.; Wu, H. Q.; Lu, Z. Y.; Sun, W.; Hu, Y. H. The flotation and adsorption of mixed collectors on oxide and silicate minerals. *Adv. Colloid Interface Sci.* **2017**, 250, 1–14.
- (12) Li, Y.; Wei, M. L.; Liu, L.; Xue, Q.; Yu, B. W. Adsorption of toluene on various natural soils: Influences of soil properties, mechanisms, and model. *Sci. Total Environ.* **2020**, *740*, 140104.
- (13) Silva, L. A.; Garrot, T. G.; Pereira, A. M.; Correia, J. C. G. Historical perspective and bibliometric analysis of molecular modeling applied in mineral flotation systems. *Minerals Engineering* **2021**, *170*, 107062.
- (14) Sun, W. H.; Liu, W. G.; Dai, S. J.; Duan, H.; Liu, W. B. Inserting EO groups to improve the performance of fatty acid collectors: Flotation and adsorption study performed with calcite, dolomite, and quartz. Sep. Purif. Technol. 2021, 272, 118952.
- (15) Wu, H. Q.; Tian, J.; Xu, L. H.; Wang, Z. J.; Xu, Y. B.; Gao, Z. Y.; Sun, W.; Hu, Y. H. Anisotropic surface chemistry properties of salt-type and oxide mineral crystals. *Minerals Engineering* **2020**, *154*, 106411.
- (16) Liu, W. P.; Wang, Z. X.; Wang, X. M.; Miller, J. D. Smithsonite flotation with lauryl phosphate. *Minerals Engineering* **2020**, 147, 106155.
- (17) Shrimali, K.; Yin, X. H.; Wang, X. M.; Miller, J. D. Fundamental issues on the influence of starch in amine adsorption by quartz. Colloids and Surfaces a-Physicochemical and Engineering Aspects 2017, 522, 642–651.
- (18) Zhu, G. L.; Wang, X. M.; Li, E. Z.; Wang, Y. H.; Miller, J. D. Wetting characteristics of spodumene surfaces as influenced by collector adsorption. *Minerals Engineering* **2019**, *130*, 117–128.
- (19) Wanhala, A. K.; Doughty, B.; Bryantsev, V. S.; Wu, L.; Mahurin, S. M.; Jansone-Popova, S.; Cheshire, M. C.; Navrotsky, A.; Stack, A. G. Adsorption mechanism of alkyl hydroxamic acid onto bastnasite: Fundamental steps toward rational collector design for rare earth elements. *J. Colloid Interface Sci.* **2019**, *553*, 210–219.
- (20) Sutton, J. E.; Roy, S.; Chowdhury, A. U.; Wu, L.; Wanhala, A. K.; De Silva, N.; Jansone-Popova, S.; Hay, B. P.; Cheshire, M. C.; Windus, T. L.; Stack, A. G.; Navrotsky, A.; Moyer, B. A.; Doughty, B.; Bryantsev, V. S. Molecular Recognition at Mineral Interfaces: Implications for the Beneficiation of Rare Earth Ores. ACS Appl. Mater. Interfaces 2020, 12 (14), 16327–16341.
- (21) Kijjanapanich, P.; Annachhatre, A. P.; Esposito, G.; Lens, P. N.L. Use of organic substrates as electron donors for biological sulfate reduction in gypsferous mine soils from Nakhon Si Thammarat (Thailand). *Chemosphere* **2014**, *101*, 1–7.
- (22) Perry, E.; Velazquez-Oliman, G.; Marin, L. The hydrogeochemistry of the karst aquifer system of the northern Yucatan

- Peninsula, Mexico. International Geology Review 2002, 44 (3), 191–221.
- (23) Zhang, D.; Li, X. D.; Zhao, Z. Q.; Liu, C. Q. Using dual isotopic data to track the sources and behaviors of dissolved sulfate in the western North China Plain. *Appl. Geochem.* **2015**, *52*, 43–56.
- (24) Matin, A.; Rahman, F.; Shafi, H. Z.; Zubair, S. M. Scaling of reverse osmosis membranes used in water desalination: Phenomena, impact and control; future directions. *Desalinaton* **2019**, *455*, 135–157.
- (25) Fipps, G. Irrigation Water Quality Standards and Salinity Management Strategies; Texas A&M: College Station, TX, 2003.
- (26) Sharma, M. K.; Kumar, M. Sulphate contamination in groundwater and its remediation: an overview. *Environmental Monitoring and Assessment* **2020**, 192 (2), 74.
- (27) Anderson, G. C.; Pathan, S.; Easton, J.; Hall, D. J. M.; Sharma, R. Short- and Long-Term Effects of Lime and Gypsum Applications on Acid Soils in a Water-Limited Environment: 2. Soil Chemical Properties. *Agronomy-Basel* **2020**, *10* (12), 1987.
- (28) Anderson, G. C.; Pathan, S.; Hall, D. J. M.; Sharma, R.; Easton, J. Short- and Long-Term Effects of Lime and Gypsum Applications on Acid Soils in a Water-Limited Environment: 3. Soil Solution Chemistry. *Agronomy-Basel* **2021**, *11* (5), 826.
- (29) Sharma, H.; Dufour, S.; Arachchilage, G. W. P. P.; Weerasooriya, U.; Pope, G. A.; Mohanty, K. Alternative alkalis for ASP flooding in anhydrite containing oil reservoirs. *Fuel* **2015**, *140*, 407–420
- (30) Xu, Y.; Liao, Y.; Lin, Z.; Lin, J.; Li, Q.; Lin, J.; Jin, Z. Precipitation of calcium sulfate dihydrate in the presence of fulvic acid and magnesium ion. *Chemical Engineering Journal* **2019**, 361, 1078–1088
- (31) Felmy, A. R.; Rai, D.; Amonette, J. E. The solubility of Barite and celestite in sodium-sulfate evaluation of thermodynamic data. *J. Solution Chem.* **1990**, *19* (2), 175–185.
- (32) Monnin, C.; Galinier, C. The solubility of celestite and Barite in electrolyte-solutions and natural waters at 25°C a thermodynamic study. *Chem. Geol.* **1988**, *71* (4), 283–296.
- (33) Garcia, J.; Schultz, L. D. Determination of Sulfate by Conductometric Titration: An Undergraduate Laboratory Experiment. *Journal of Chemical Education* **2016**, 93, 910–914.
- (34) Lambert, A. G.; Davies, P. B.; Neivandt, D. J. Implementing the theory of sum frequency generation vibrational spectroscopy: A tutorial review. *Appl. Spectrosc. Rev.* **2005**, *40* (2), 103–145.
- (35) Vidal, F.; Tadjeddine, A. Sum-frequency generation spectroscopy of interfaces. *Rep. Prog. Phys.* **2005**, *68* (5), 1095–1127.
- (36) Wang, H. F.; Gan, W.; Lu, R.; Rao, Y.; Wu, B. H. Quantitative spectral and orientational analysis in surface sum frequency generation vibrational spectroscopy (SFG-VS). *Int. Rev. Phys. Chem.* **2005**, 24 (2), 191–256.
- (37) Can, S. Z.; Mago, D. D.; Walker, R. A. Structure and organization of hexadecanol isomers adsorbed to the air/water interface. *Langmuir* **2006**, 22 (19), 8043–8049.
- (38) Karnes, J. J.; Gobrogge, E. A.; Walker, R. A.; Benjamin, I. Unusual Structure and Dynamics at Silica/Methanol and Silica/Ethanol Interfaces-A Molecular Dynamics and Nonlinear Optical Study. *J. Phys. Chem. B* **2016**, *120* (8), 1569–1578.
- (39) Link, K. A.; Hsieh, C. Y.; Tuladhar, A.; Chase, Z.; Wang, Z. M.; Wang, H. F.; Walker, R. A. Vibrational studies of saccharide-induced lipid film reorganization at aqueous/air interfaces. *Chem. Phys.* **2018**, *512*, 104–110.
- (40) Esenturk, O.; Walker, R. A. Surface vibrational structure at alkane liquid/vapor interfaces. *J. Chem. Phys.* **2006**, *125*, 174701.
- (41) Koroleva, M. Y.; Karakatenko, E. Y.; Yurtov, E. V. Synthesis of hydroxyapatite nanoparticles by controlled precipitation in the presence of sodium docecyl sulfate. *Colloid J.* **2020**, *82*, 275–283.
- (42) Zhang, P.; Xiang, M. X.; Li, P.; Ouyang, S. D.; He, T.; Deng, Q. The enhancement roles of sulfate on the adsorption of sodium dodecylsulfate by calcium-based layered double hydroxide: microstructure and thermal behaviors. *Environ. Sci. Pollut. Res.* **2019**, 26, 19320–19326.

- (43) Baviere, M.; Bazin, B.; Aude, R. Calcium effect on the solubility of sodium dodecyl-sulfate in sodium-chloride solutions. *J. Colloid Interface Sci.* 1983, 92 (2), 580–583.
- (44) Macphail, R. A.; Strauss, H. L.; Snyder, R. G.; Elliger, C. A. C-H Stretching modes and the sructure of normal-alkyl chains. 2. Long, all-trans chains. *J. Phys. Chem.* **1984**, *88* (3), 334–341.
- (45) Snyder, R. G.; Strauss, H. L.; Elliger, C. A. C-H Stretching modes and the sructure of normal-alkyl chains. 1. Long, disordered chains. *J. Phys. Chem.* **1982**, *86* (26), 5145–5150.
- (46) Conboy, J. C.; Messmer, M. C.; Richmond, G. L. Dependence of alkyl chain conformation of simple ionic surfactants on head group functionality as studied by vibrational sum-frequency spectroscopy. *J. Phys. Chem. B* **1997**, *101* (34), 6724–6733.
- (47) Brindza, M. R.; Ding, F.; Fourkas, J. T.; Walker, R. A. n-alkane adsorption to polar silica surfaces. *J. Chem. Phys.* **2010**, *132*, 114701.
- (48) Kryachko, E. S.; Zeegers-Huyskens, T. Theoretical study of the CH ···X- interaction of fluoromethanes and chloromethanes with fluoride, chloride, and hydroxide anions. *J. Phys. Chem. A* **2002**, *106* (29), 6832–6838.
- (49) Fourkas, J. T.; Walker, R. A.; Can, S. Z.; Gershgoren, E. Effects of reorientation in vibrational sum-frequency spectroscopy. *J. Phys. Chem. C* **2007**, *111* (25), 8902–8915.